Controlling Majorana modes by *p*-wave pairing in two-dimensional $p + id$ topological superconductors

Morten Amundsen [1] and Vladimir Juričić [1,2]

[1]*Nordita, KTH Royal Institute of Technology and Stockholm University, Hannes Alfvéns väg 12, SE-106 91 Stockholm, Sweden*
[2]*Departamento de Física, Universidad Técnica Federico Santa María, Casilla 110, Valparaíso, Chile*

(Received 27 August 2021; revised 16 December 2021; accepted 20 December 2021; published 3 February 2022)

We show that corner Majorana zero modes in a two-dimensional $p + id$ topological superconductor can be controlled by the manipulation of the parent p-wave superconducting order. Assuming that the p-wave superconducting order is in either a chiral or helical phase, we find that when a $d_{x^2-y^2}$ wave superconducting order is induced, the system exhibits quite different behavior depending on the nature of the parent p-wave phase. In particular, we find that while in the helical phase, a localized Majorana mode appears at each of the four corners, in the chiral phase, it is localized along only two of the four edges. We furthermore demonstrate that the Majoranas can be directly controlled by the form of the edges, as we explicitly show in the case of circular edges. We argue that the application of strain may provide additional means of fine-tuning the Majorana zero modes in the system; in particular, it can partially gap them out. Our findings may be relevant for probing the topology in two-dimensional mixed-pairing superconductors.

DOI: 10.1103/PhysRevResearch.4.013088

I. INTRODUCTION

Majorana zero modes (MZMs) represent a hallmark feature of topological superconductivity with several interesting properties [1–8]. In addition to their fundamental importance, MZMs are fascinating because they exhibit non-Abelian statistics, which manifests in braiding operations. This could be of crucial importance for future applications, for instance, in information technology [9–12], and has been the subject of intense research [13–23]. MZMs appear as topologically protected boundary states at interfaces where the topological invariant changes, while the bulk remains gapped. Typically, a topological superconductor (SC) features MZMs at interfaces of codimension $m = 1$, imprinting the standard topological bulk-boundary correspondence [3,4]. In a one-dimensional finite system, they take the form of localized modes at the ends, while in two and three dimensions they are realized as, respectively, edge and surface states.

New platforms for the realization of MZMs have recently appeared with the advent of higher-order topological states [24–34] which generalize the standard bulk-boundary correspondence. Within this class of states, higher-order topological SCs can localize MZMs at interfaces of codimension $m > 1$. In particular, two- (three-) dimensional second- (third-) order topological SCs may host corner MZMs [35–68] with codimension $m = d$ in d spatial dimensions. In a two-dimensional (2D) topological state with an insulating or superconducting bulk gap, the corner zero modes can be obtained by gapping out the first-order edge states with a mass term that features a domain wall in momentum space, realizing a special case of the hierarchy of higher-order topological states [31,69]. In this respect, several concrete ways to realize corner MZMs in two dimensions have been proposed so far, for instance, by inducing a superconducting gap for the edge states of a topological insulator, either intrinsically [55] or via the proximity effect [35,38,40,56,58–60]. It has also been shown that they may emerge when pairing of an appropriate symmetry is combined with a spin-dependent field, such as spin-orbit coupling [41,61,62]. Furthermore, several works recently proposed means by which the order of a topological superconductor may be manipulated, along with the position of the resulting corner MZMs. Indeed, a first-order topological SC may be promoted to second order by the application of a magnetic field, with the location of the corner modes determined by the orientation of the field [39,50,63]. It has also been theoretically shown that second-order topological superconductivity can emerge in Josephson junctions, in which case the phase difference between the SCs provides additional means of manipulation [64,65].

We here consider a different scenario in which a variety of MZMs can be generated solely by manipulating the parent p-wave superconducting order in a mixed-parity $p + id$ 2D SC. We assume that the p-wave superconducting order, in the absence of any other pairing, hosts a first-order topological state and exists in either a chiral or helical phase, referring to whether it breaks or preserves time-reversal symmetry, respectively. We show that when a $d_{x^2-y^2}$-wave superconducting order is induced, e.g., via the proximity effect, the system exhibits quite different behavior depending on the parent p-wave phase. In particular, we find that in the helical phase, a localized Majorana mode appears at each of the four corners,

as shown in Fig. 1. In the chiral phase, on the other hand, no corner modes appear. Instead, a gap emerges in two out of the four edge modes (Fig. 2). Therefore, the behavior of the Majorana modes can be tuned solely by manipulating the pairing symmetry of the parent topological SC. As we show, the edge geometry can also be relevant in this regard; see Fig. 3 where we display the Majorana states for a circular edge geometry. Finally, we demonstrate that the application of strain may drive a topological phase transition when the parent phase is chiral. As a result, the strain gaps out two out of the four edges, as displayed in Fig. 4.

The rest of this paper is organized as follows. In Sec. II we introduce the model for the $p+id$ topological SC we consider. Next, we present analytical arguments for the behavior of the resulting edge states in Sec. III, before moving on to discussing the numerical results in Sec. IV. Finally, we analyze the effect of strain in Sec. V and present our conclusions together with an outlook in Sec. VI.

II. MODEL

We employ the standard Bogoliubov–de Gennes formalism to study the system, with the Hamiltonian given as

$$H = \frac{1}{2}\sum_{\mathbf{k}} \psi_{\mathbf{k}}^{\dagger}\hat{H}(\mathbf{k})\psi_{\mathbf{k}}, \tag{1}$$

where the corresponding Nambu spinor is $\psi_{\mathbf{k}} = (c_{\mathbf{k}\uparrow} \quad c_{\mathbf{k}\downarrow} \quad c^{\dagger}_{-\mathbf{k}\uparrow} \quad c^{\dagger}_{-\mathbf{k}\downarrow})^{\top}$, with $c_{\mathbf{k}\uparrow}$ ($c^{\dagger}_{\mathbf{k}\downarrow}$) being the annihilation (creation) operator for the quasiparticle with spin up (down) and momentum $\mathbf{k}$. Here,

$$\hat{H} = \begin{pmatrix} h(\boldsymbol{k}) & \Delta(\boldsymbol{k}) \\ -\Delta^{*}(-\boldsymbol{k}) & -h^{*}(-\boldsymbol{k}) \end{pmatrix}, \tag{2}$$

with the blocks describing the normal (nonsuperconducting) state and the pairing given by, respectively,

$$h(\boldsymbol{k}) = \left(\frac{\hbar^2\boldsymbol{k}^2}{2m} - \mu\right)\sigma_0 \equiv \xi_k\sigma_0, \tag{3}$$

$$\Delta(\boldsymbol{k}) = \left[\frac{\Delta_p}{k_{\mathrm{F}}}\boldsymbol{g}(\boldsymbol{k})\cdot\boldsymbol{\sigma} + \frac{i\Delta_d}{k_{\mathrm{F}}^2}\left(k_x^2 - k_y^2\right)\right]i\sigma_2, \tag{4}$$

where μ is the chemical potential, m is the quasiparticle mass, and the Pauli matrices $\boldsymbol{\sigma}$ and the unit 2×2 matrix σ_0 act in the spin space, k_F is the Fermi momentum. Here, Δ_p and Δ_d are the amplitudes of the p- and d-wave superconducting orders. For the latter we choose the $d_{x^2-y^2}$ component $\sim (k_x^2 - k_y^2)$ as it features domain walls along the diagonals in momentum space, located at $k_x = \pm k_y$, where it changes sign, thereby *partially* gapping out the edge states [70]. We also include a relative phase of $\pi/2$ between the two order parameters, implying that the mixed-pairing state breaks time-reversal symmetry. Notice, however, that the d-wave component preserves the product of the C_4 rotational and time-reversal ($\mathcal{T}$) symmetries, $C_{4T} = C_4\mathcal{T}$, implying that the resulting $p+id$ superconducting state may feature the same composite symmetry. This, indeed, occurs when the p-wave component is helical (see below), in which case also a Z_2 topological invariant protects the resulting second-order topological SC [35]. The vector $\boldsymbol{g}(\boldsymbol{k})$ parametrizes the triplet p-wave superconducting paring and takes the form

$$\boldsymbol{g}(\boldsymbol{k}) = \cos\theta\ \boldsymbol{k}\times\hat{z} + \sin\theta(k_x + ik_y)\hat{z}, \tag{5}$$

where $\hat{z}$ is the unit vector pointing in the z direction, assumed to be normal to the 2D plane. The helical phase is found by setting $\theta = 0$ and represents a time-reversal invariant SC, featuring a pair of counterpropagating gapless Majorana edge modes. On the other hand, the chiral phase, which breaks the time-reversal symmetry, is found for $\theta = \pi/2$. In the following we are interested only in these two special cases and also refer to the mixed $p+id$ state as either chiral or helical depending upon the phase of the parent p-wave component. Since we consider only the topological regime, we do not include the s-wave pairing in the Hamiltonian in Eq. (2).

The bulk spectrum of the Hamiltonian in Eqs. (2)–(4) is given as

$$E(\boldsymbol{k}) = \pm\sqrt{\xi_k^2 + a_+\Delta_p^2 + a_-^2\Delta_d^2 \pm 2\Delta_p\frac{k_y}{k_{\mathrm{F}}}b(\theta)}, \tag{6}$$

with $a_{\pm} \equiv a_{\pm}(\boldsymbol{k}) = (k_x^2 \pm k_y^2)/k_{\mathrm{F}}^2$, and

$$b(\theta) = \sin\theta\sqrt{a_-^2\Delta_d^2 + a_+\Delta_p^2\cos^2\theta}.$$

The spectrum for the helical ($\theta = 0$) and chiral ($\theta = \pi/2$) phases thus reduces to

$$E(\boldsymbol{k}) = \begin{cases} \pm\sqrt{\xi_k^2 + a_+\Delta_p^2 + a_-^2\Delta_d^2}, & \theta = 0, \\ \pm\sqrt{\xi_k^2 + \frac{k_x^2}{k_{\mathrm{F}}^2}\Delta_p^2 + \left(a_-\Delta_d \pm \frac{k_y}{k_{\mathrm{F}}}\Delta_p\right)^2}, & \theta = \frac{\pi}{2}. \end{cases}$$

It is clear that for $\theta = 0$, the bulk band structure always features a gap, as long as $\Delta_p \neq 0$. The same holds for $\theta = \frac{\pi}{2}$, except for the critical value of $\Delta_d = \Delta_p$, where the gap closes. We furthermore note that both of the gapped regions $\Delta_d < \Delta_p$ and $\Delta_d > \Delta_p$ are topologically nontrivial and feature gapless edge states, which will be evident in the following.

III. ANALYTICAL RESULTS

To understand the effects of the d-wave superconducting order on the edge states present in this system, we introduce an interface which is oriented with an angle α with respect to the horizontal (x) principal crystalline axis. The Hamiltonian in this rotated coordinate system, $\boldsymbol{k} = (k_x, k_y) \to \boldsymbol{k}' = (k_{||}, k_{\perp})$, is given by

$$\hat{H}'(\boldsymbol{k}') = \hat{R}\hat{H}(\mathcal{R}^{-1}\boldsymbol{k}')\hat{R}^{\dagger}, \tag{7}$$

where

$$\hat{R}(\alpha) = \begin{pmatrix} R(\alpha) & 0 \\ 0 & R^{*}(\alpha) \end{pmatrix} \tag{8}$$

is the rotation operator in the Nambu basis defined in Eq. (1) and $R = \exp[i\alpha\sigma_3/2]$ represents the operator of the rotation by the angle α about the z axis in the spin-1/2 representation. The momenta $\boldsymbol{k}'$ and $\boldsymbol{k}$ are related by a rotation about the z axis with the same angle α, $\boldsymbol{k}' = \mathcal{R}(\alpha)\boldsymbol{k}$, with the rotational matrix given by

$$\mathcal{R}(\alpha) = \begin{pmatrix} \cos\alpha & \sin\alpha \\ -\sin\alpha & \cos\alpha \end{pmatrix}. \tag{9}$$

The corresponding edge Hamiltonian is then obtained by projecting a part of the rotated bulk Hamiltonian $\hat{H}'(\boldsymbol{k}')$ [Eq. (7)] *not* used to obtain the zero modes onto the subspace spanned by the zero-energy edge modes.

In the following, we assume that both Δ_p and Δ_d are much smaller than the Fermi energy (weak-pairing limit), which we set equal to the chemical potential, $\mu = \hbar^2 k_{\rm F}^2/2m$. In addition, we assume that the wave vector parallel to the interface is much smaller than the Fermi momentum, $k_{||} \ll k_{\rm F}$. To find the form of the edge Hamiltonian, as previously announced, we first perform the rotation in Eq. (7) and then solve for the zero-energy modes in the absence of the d-wave pairing. To this end, in the rotated Hamiltonian (2), we isolate a part that is proportional to Δ_p and depends on $k_\perp$, the wave vector orthogonal to the interface. The total Hamiltonian therefore acquires the form

$$\hat{H}'(\mathbf{k}') = \hat{H}'_0(k_\perp) + \hat{H}'_1(k_\parallel) + \hat{H}'_2(k_\perp, k_\parallel), \tag{10}$$

with

$$\hat{H}'_0(k_\perp) \simeq \frac{\hbar^2}{2m}\left(k_\perp^2 - k_{\rm F}^2\right)\tau_3\sigma_0 - \frac{k_\perp}{k_{\rm F}}\Delta_p(\tau_2\sigma_0\cos\theta - e^{i\alpha\tau_3\sigma_0}\tau_1\sigma_1\sin\theta), \tag{11}$$

$$\hat{H}'_1(k_\parallel) = \frac{k_{||}}{k_{\rm F}}\Delta_p(\tau_1\sigma_3\cos\theta - e^{i\alpha\tau_3\sigma_0}\tau_2\sigma_1\sin\theta), \tag{12}$$

$$\hat{H}'_2(k_\perp, k_\parallel) = -\frac{\Delta_d}{k_F^2}[(k_{||}^2 - k_\perp^2)\cos 2\alpha - 2k_{||}k_\perp \sin 2\alpha]\tau_1\sigma_2. \tag{13}$$

Here, $\tau_a\sigma_b \equiv \tau_a \otimes \sigma_b$ is a Kronecker product between Pauli matrices in Nambu and spin space. Since the edge breaks translation invariance, we make the substitution $k_\perp \to -i\partial_{r_\perp}$, where $r_\perp$ is the direction orthogonal to the edge, and solve the resulting differential equation with the boundary conditions $\psi(r_\perp = 0) = \psi(r_\perp = \infty) = 0$. The unperturbed Hamiltonian, given by Eq. (11), admits two degenerate zero-energy eigenstates of the form

$$\psi_a(r_\perp) = \sqrt{2\kappa}\; e^{-\kappa r_\perp}\sin k_{\rm F} r_\perp\; \varphi_a, \tag{14}$$

with $a = 1, 2$, the spinors

$$\varphi_1 = (-i\cos\theta \quad e^{i\alpha}\sin\theta \quad -i \quad 0)^\top,$$
$$\varphi_2 = (e^{i\alpha}\sin\theta \quad -i\cos\theta \quad 0 \quad -i)^\top,$$

and $\kappa = m\Delta_p/(\hbar^2 k_F)$. The effective Hamiltonian for the edge states is thus found, to first order in the perturbation expansion, as the projection

$$H^e_{ab}(\theta) = \int_0^\infty dr_\perp\; \psi_a^\dagger(r_\perp)(\hat{H}'_1 + \hat{H}'_2)\psi_b(r_\perp), \tag{15}$$

which gives

$$H^e(\theta) = -\Delta_p\frac{k_{||}}{k_{\rm F}}\begin{pmatrix} 1 & -\frac{i}{2}e^{i\alpha}\sin 2\theta \\ \frac{i}{2}e^{-i\alpha}\sin 2\theta & -\cos 2\theta \end{pmatrix} - \Delta_d\cos 2\alpha\begin{pmatrix} \sin\theta\cos\alpha & i\cos\theta \\ -i\cos\theta & -\sin\theta\cos\alpha \end{pmatrix}, \tag{16}$$

where we have kept only the leading term in Eq. (13). The term $\sim k_\parallel$ in Eq. (13) vanishes identically after taking the projection (15), and we have neglected the term $\sim k_\parallel^2$ as being less relevant by power counting than the leading one in the low-energy edge Hamiltonian. Note that this term can be, in principle, included in this Hamiltonian following the outlined procedure.

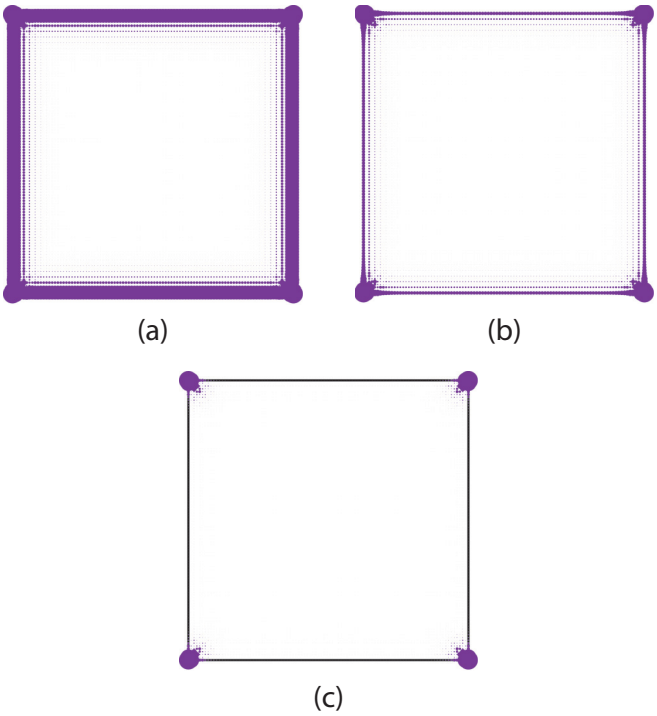

FIG. 1. Local density of states at zero energy $\nu(0)$ in the helical phase ($\theta = 0$), with the d-wave order parameter set to (a) $\Delta_d = 0$, (b) $\Delta_d = 0.1\Delta_p$, and (c) $\Delta_d = 0.2\Delta_p$. The dot size at a particular point indicates the size of $\nu(0)$ at that point. In all plots, we use the Hamiltonian in Eq. (19) and set $\mu = 2t$, $\Delta_p = t = 1$, and $a = 1$. The system size is 100×100 sites.

The first term in Eq. (16) describes the Majorana edge modes, having a characteristic nodal structure in $k_\parallel$ in the absence of the d-wave pairing. These modes are, in turn, gapped by the d-wave pairing term. For $\theta = 0$ (the helical phase), one thus obtains

$$H^e(\theta = 0) = \begin{pmatrix} -\Delta_p\frac{k_{||}}{k_{\rm F}} & i\Delta_d\cos 2\alpha \\ -i\Delta_d\cos 2\alpha & \Delta_p\frac{k_{||}}{k_{\rm F}} \end{pmatrix}. \tag{17}$$

Clearly, a mass term proportional to $\cos 2\alpha$ appears, having domain walls along the two diagonals, located at $\alpha = \pm\pi/4$. Hence, the edge modes are gapped out, and only the corner modes remain, in agreement with Refs. [35,36]. These corner MZMs are protected by the composite C_{4T} symmetry and a Z_2 topological invariant [see also the discussion after Eq. (4)].

In the chiral phase, for $\theta = \pi/2$, we do not have a band crossing which may turn into an anticrossing and open up a gap at the edge. In this case Eq. (16) takes the form

$$H^e\left(\theta = \frac{\pi}{2}\right) = -\Delta_p\frac{k_{||}}{k_F}\sigma_0 - \Delta_d\cos\alpha\cos 2\alpha\;\sigma_3, \tag{18}$$

which suggests that the presence of the d wave order parameter has only a trivial effect on the edge states in the regime $\Delta_d < \Delta_p$. However, the closing of the bulk gap at $\Delta_d = \Delta_p$

signals a possible phase transition, and therefore, something interesting may occur also in this system. It turns out that a *selective gapping* of the edge states is possible for $\Delta_d > \Delta_p$, as can already be seen from Eq. (18). Namely, by taking the values of the angle $\alpha = 0$ ($\alpha = \pi/2$), corresponding to horizontal (vertical) edge, we find that the horizontal and vertical edges should be gapped and gapless, respectively. This is exactly what we find by numerical means, as shown in the next section.

IV. NUMERICAL ANALYSIS

In addition to the analytical analysis presented in the previous section, we also numerically study the $p + id$ SC described by Eqs. (2)–(4). The corresponding square-lattice Hamiltonian reads

$$H = \frac{1}{2}\sum_{jl} \psi_j^\dagger \hat{H}_{jl} \psi_l, \tag{19}$$

with the Nambu vector at lattice site j, $\psi_j = (c_{j\uparrow} \quad c_{j\downarrow} \quad c_{j\uparrow}^\dagger \quad c_{j\downarrow}^\dagger)^\top$, and $\hat{H} = \hat{H}_0 + \hat{H}_p + \hat{H}_d$, where

$$\hat{H}_0 = [-t(\delta_{\hat{x}} + \delta_{-\hat{x}} + \delta_{\hat{y}} + \delta_{-\hat{y}}) + (4t - \mu)\delta_{jl}]\tau_3\sigma_0, \tag{20}$$

$$\hat{H}_p = \frac{\Delta_p}{2ik_F a}\{[(\delta_{\hat{y}} - \delta_{-\hat{y}})\tau_1\sigma_3 - (\delta_{\hat{x}} - \delta_{-\hat{x}})\tau_2\sigma_0]\cos\theta + [(\delta_{\hat{x}} - \delta_{-\hat{x}})\tau_1\sigma_1 - (\delta_{\hat{y}} - \delta_{-\hat{y}})\tau_2\sigma_1]\sin\theta\}, \tag{21}$$

$$\hat{H}_d = \frac{\Delta_d}{k_F^2 a^2}[\delta_{\hat{x}} + \delta_{-\hat{x}} - \delta_{\hat{y}} - \delta_{-\hat{y}}]\tau_1\sigma_2. \tag{22}$$

In the above, $t = \hbar^2/2ma^2$, and we use the shorthand notation $\delta_{\hat{n}} \equiv \delta_{j+\hat{n},l}$. We furthermore remark that the momentum space representation of the above lattice Hamiltonian with periodic boundary conditions is found from Eqs. (2)–(4) by replacing

$$\xi_k \to -2t(\cos k_x a + \cos k_y a) + 4t - \mu, \quad \boldsymbol{k} \to \frac{1}{a}\sin(\boldsymbol{k}a)$$

and substituting

$$k_x^2 - k_y^2 \to \frac{2}{a^2}(\cos k_x a - \cos k_y a)$$

in the d-wave component of the superconducting order parameter. This has the effect of shifting the location at which the bulk gap closes, which is a characteristic feature of the chiral phase, to

$$\Delta_d = \Delta_p\sqrt{1 - \frac{\mu}{4t}} \equiv \Delta_d^c. \tag{23}$$

Furthermore, with $\mu/t = k_F^2 a^2$, it is clear that the above discretized model becomes equivalent to its continuum counterpart in the limit $k_F a \ll 1$.

We now consider the edge states in a square-lattice system. We compute the local density of states at site position j as

$$\nu_j(E) = \sum_n |v_{n,j}|^2 \delta(E - E_n) \simeq \frac{1}{\sqrt{\pi\lambda}}\sum_n |v_{n,j}|^2 e^{-(E-E_n)^2/\lambda}, \tag{24}$$

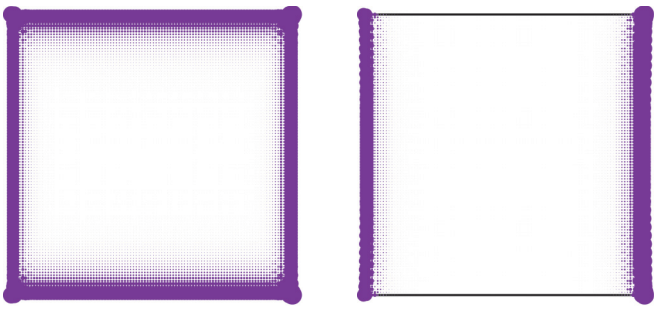

FIG. 2. The local density of states in the chiral phase ($\theta = \frac{\pi}{2}$) in the two regimes separated by the critical value of the d-wave order parameter Δ_d^c, at which the bulk gap closes. In (a) $\Delta_d = 0.5\Delta_d^c$, whereas in (b) $\Delta_d = 1.5\Delta_d^c$. The dot size at a particular point indicates the size of $\nu(0)$ at that point. In both plots, we use the Hamiltonian in Eq. (19) and set $\mu = 2t$, $\Delta_p = t = 1$, and $a = 1$. The system size is 100×100 sites.

where E_n are the eigenvalues of the Hamiltonian and $v_{n,j}$ are the values of the corresponding eigenvectors at j. The broadening parameter λ is set to 5×10^{-3}. In the helical phase, as shown in Fig. 1, the edge states quickly vanish with increasing Δ_d, becoming completely gapped out at $\Delta_d = 0.2\Delta_p$ and thus leaving only the corner modes.

We turn to the chiral phase, where the gap closing at $\Delta_d = \Delta_d^c$ separates two regions of interest. The region with $\Delta_d < \Delta_d^c$ is topologically equivalent to the case where $\Delta_d = 0$, and we thus expect that the results from Eq. (16) apply here, implying that the d-wave order parameter does not gap out the chiral edge states. This is indeed found to be the case in our numerical analysis, as illustrated in Fig. 2(a), in which the local density of states at $\Delta_d = t/2\sqrt{2} = 0.5\Delta_d^c$ is shown. In contrast, for $\Delta_d = 3t/2\sqrt{2} = 1.5\Delta_d^c$, shown in Fig. 2(b), the behavior is different. In that case the horizontal edges are gapped out, but the vertical edge states remain gapless, in agreement with Eq. (18). We furthermore note that a phase shift of $\pi/2$ in the relative phase between Δ_d and Δ_p would amount to a $\pi/2$ rotation of the result in Fig. 2(b). Therefore, the relative phase between the two pairing order parameters translates into the pattern of the gap at the edge of the system.

We now investigate the edge states in the case of a disk geometry. This is relevant because the behavior of the edge states for any polygonal geometry may immediately be deduced by comparing the corner opening angles with corresponding points on the circle. The modeling of the disk is performed by creating a square grid and discarding all nodes which fall outside a selected radius, here chosen to be 60 nodes. The results are shown in Fig. 3 for increasing values of Δ_d above the critical value Δ_d^c. Below Δ_d^c (not shown), the edge states are uniformly distributed around the entire edge, as expected. Immediately after crossing the critical value, a gap is opened up in the edge states at angles around $\gamma = \{\pi/2, 3\pi/2\}$, as shown in Fig. 3(a) for $\Delta_d = 1.5\Delta_d^c$, and γ is the polar angle of the circle. This is consistent with the partial gapping of the edge states observed in Fig. 2(b), which probes the same angles, along with the angles $\{0, \pi\}$, which are gapless. A

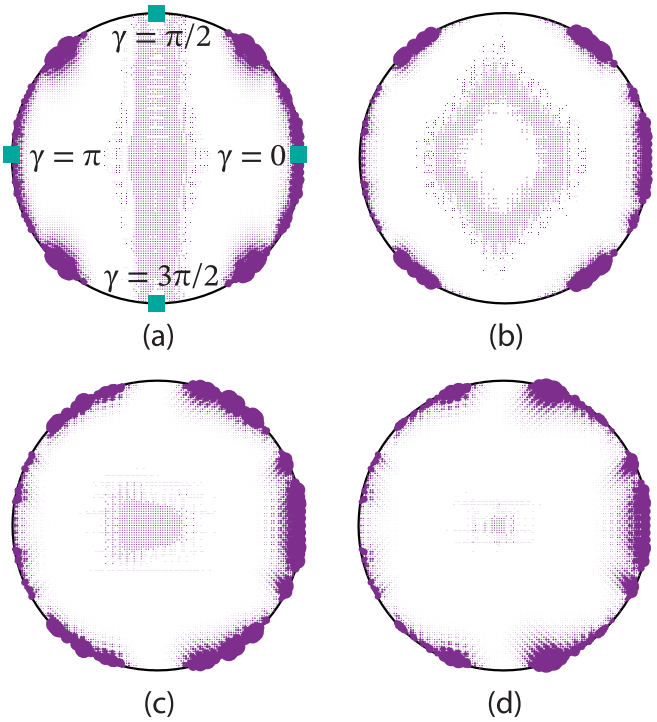

FIG. 3. The edge states in a circular geometry when the system is in the chiral phase for increasing values of the d-wave order parameter, equal to (a) $\Delta_d = 1.5\Delta_d^c$, (b) $\Delta_d = 3\Delta_d^c$, (c) $\Delta_d = 4.5\Delta_d^c$, and (d) $\Delta_d = 6\Delta_d^c$. The squares in (a) indicate the opening angles probed by the square geometry shown in Fig. 2. The dot size at a particular point indicates the size of $\nu(0)$ at that point. In all plots we have set $\mu = 2t$, $\Delta_p = t = 1$, and $a = 1$ in the Hamiltonian in Eq. (19). The system consists of a disk with a radius of 60 sites.

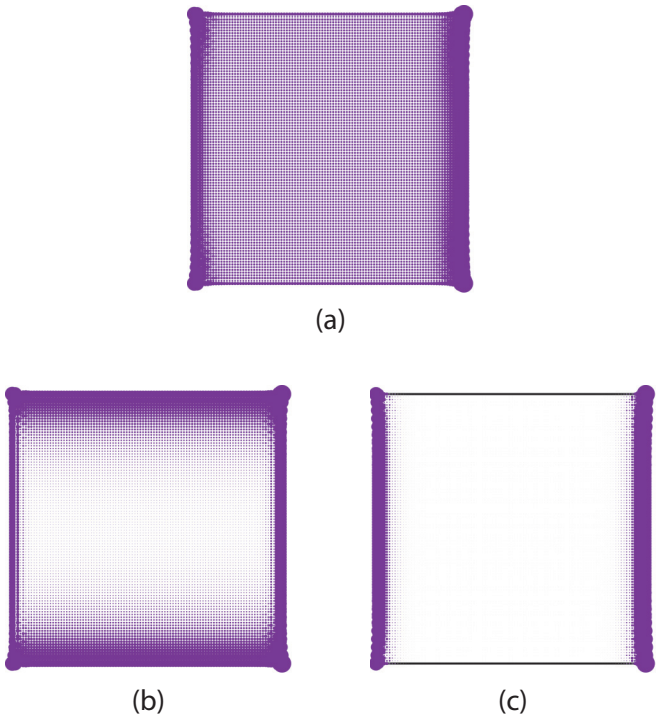

FIG. 4. The effect of strain on the zero-energy edge states in the chiral phase. In (a) the local density of states at zero energy is shown at $\Delta_d = \Delta_d^c$ without any strain. In (b) and (c) the same system is shown for an applied uniaxial strain of $\varepsilon_{xx} = 10\%$ and $\varepsilon_{yy} = 10\%$, respectively. The dot size at a particular point indicates the size of $\nu(0)$ at that point. In all plots, we set $\mu = 2t$, $\Delta_p = t = 1$, and $a = 1$ in the Hamiltonian in Eq. (19). The system size is 100×100 sites.

further increase in Δ_d increases the modulation of the density of states along the edge and produces additional gapped regions, as can be seen in Figs. 3(b)–3(d), which correspond to $\Delta_d/\Delta_d^c = 3$, 4.5, and 6, respectively. Furthermore, the gapped circle sector surrounding $\gamma = \{\pi/2, 3\pi/2\}$ is seen to narrow as Δ_d becomes larger but never closes completely, consistent with the domain wall structure of the $d_{x^2-y^2}$-wave pairing.

V. THE EFFECT OF STRAIN

We investigate strain as a potential means to manipulate the edge states. We model its effects by introducing a small strain field to the system,

$$\varepsilon = \begin{pmatrix} \varepsilon_{xx} & \varepsilon_{xy} \\ \varepsilon_{yx} & \varepsilon_{yy} \end{pmatrix}. \tag{25}$$

Here, ε_{xx} and ε_{yy} represent axial strain, defined as being positive for tensile strain, and $\varepsilon_{xy} = \varepsilon_{yx}$ represents shear strain. In the presence of such a strain field, the spatial coordinates transform as $r_i' = (\delta_{ij} + \varepsilon_{ij})r_j$, which implies that, to linear order in the strain tensor, the momentum transforms as

$$k_i' = (\delta_{ij} - \varepsilon_{ij})k_j. \tag{26}$$

By replacing $\boldsymbol{k} \to \boldsymbol{k}'$ in Eqs. (2)–(4), then inserting Eq. (26), and retaining only terms up to first order in ε, we find that additional strain-dependent terms are introduced in the Hamiltonian, which may have an effect on the edge states. For an edge with an arbitrary orientation α, the corresponding Hamiltonian, after incorporating the effects of strain, reads

$$H^e = -\Delta_p \Gamma_p(\varepsilon, \alpha)\frac{k_{||}}{k_F}\begin{pmatrix} 1 & -\frac{i}{2}e^{i\alpha}\sin 2\theta \\ \frac{i}{2}e^{-i\alpha}\sin 2\theta & -\cos 2\theta \end{pmatrix} - \Delta_d \Gamma_d(\varepsilon, \alpha)\begin{pmatrix} \sin\theta\cos\alpha & i\cos\theta \\ -i\cos\theta & -\sin\theta\cos\alpha \end{pmatrix}, \tag{27}$$

with

$$\Gamma_p(\varepsilon, \alpha) = 1 - \bar{\varepsilon} + \frac{1}{2}\delta\varepsilon\cos 2\alpha + \varepsilon_{xy}\sin 2\alpha, \tag{28}$$

$$\Gamma_d(\varepsilon, \alpha) = (1 - 2\bar{\varepsilon})\cos 2\alpha - \delta\varepsilon, \tag{29}$$

where $\bar{\varepsilon} = (\varepsilon_{xx} + \varepsilon_{yy})/2$ and $\delta\varepsilon = \varepsilon_{xx} - \varepsilon_{yy}$. We see that strain produces an effective renormalization of the p- and d-wave order parameters in the edge Hamiltonian by Γ_p and Γ_d, respectively. Furthermore, for anisotropic strain, Γ_d acquires a contribution independent of α. This implies that the corner modes in the helical phase, given by Eq. (17), can be gapped out by strain. This is also consistent with the breaking of the C_{4T} symmetry by strain, which protects the topological state. However, the gapping occurs only once the mass domain wall at the corners is removed, which requires rather large strains. For instance, with a uniaxial tensile strain of $\varepsilon_{xx} = \varepsilon$, the corner modes are gapped out for $\varepsilon > 50\%$. This is much

larger than the capacity of any known material, with graphene being the closest contender, reported to sustain strains of up to 25% [71]. In any case, these levels of strain are certainly far beyond the linear strain regime considered herein, implying the stability of the corner modes against strains in the experimentally realizable range.

In the chiral phase, we consider the effect of strain by numerical means. To this end, we replace the lattice parameter a with directionally dependent equivalents, a_x and a_y, satisfying $a_i = (1 + \varepsilon_{ii})a$. We ignore shear strain. In the regime $\Delta_d > \Delta_d^c$, we can conclude from Eq. (27) that Δ_d and Δ_p are renormalized slightly differently by strain, which agrees with the numerical analyses for $\Delta_d < \Delta_d^c$. Hence, strain may be used to change the ratio between the amplitudes of the d- and p-wave superconducting orders and thus cause a transition between the two phases exhibiting different behaviors of the edge states, which agrees with our numerical analysis. Setting $\Delta_d = \Delta_d^c$, which in the unstrained case is gapless, as shown in Fig. 4(a), we perturb the system by applying a uniaxial strain of 10% along the x and y directions, shown in Figs. 4(b) and 4(c), respectively. In the former case, it can be seen that the system is pushed into the state with uniform gapless edge modes, whereas in the latter case, the selectively gapped state is entered. Therefore, in the chiral phase, strain can be used to tune the form and the localization of the edge states.

VI. CONCLUSIONS AND OUTLOOK

In conclusion, we have studied the Majorana zero modes in a 2D SC with mixed p- and d-wave pairings, considering both the helical and chiral p-wave phases. For the parent helical p-wave order, we found that the effect of the d-wave order parameter is to gap out the edge states, leaving only zero-energy Majorana corner modes. In the case of the parent chiral p-wave pairing, we showed that the edge states can be *partially* gapped out above a critical value of the d-wave order parameter. Therefore, the parent p-wave phase can control the form of the Majorana modes in the $p + id$ topological SC. We found that the localization of the Majorana modes can also be tuned by the geometry of the edges, as implied by our results in the circular edge geometry. Moreover, the localization of the MZMs in a polygonal geometry may be inferred by identifying the opening angle of a given corner with a corresponding point on the circle. We have also investigated the effect of strain and found that the higher-order topological SC produced in the parent helical phase is robust against strain up to the experimentally reachable values. On the other hand, in the chiral phase, we showed that strain can be used to induce a transition between topologically distinct phases with gapless and partially gapped edge states. Hence, the application of strain, through the strain-induced topological phase transition, may indeed provide a direct means of manipulating the Majorana modes.

The experimental realization of such a superconducting system is a challenging issue at present, but we will nevertheless indicate a few promising avenues. First, 2D $p + id$ second-order topological SCs may be hosted in doped second-order topological insulators, as was recently advocated in Ref. [48]. Another available route is to make use of the proximity effect between a topological p-wave SC and a d-wave SC. Typical examples of the latter are cuprates such as $YBa_2Cu_3O_{7-\delta}$ [72], while the former is more difficult to find. Indeed, the leading candidate for topological p-wave superconductivity, Sr_2RuO_4, was recently shown to be most likely *not* of p-wave nature [73,74]. Intensive research is, however, still ongoing, and other potential candidates are uranium-based heavy-fermion compounds, of which UTe_2 seems to be most promising one [75].

As we are concerned here with only 2D effects, we do not have to rely on bulk superconducting properties. This broadens the choice of materials somewhat. For instance, topological superconductivity in surface states can be achieved via the Fu-Kane construction [76], whereby a conventional s-wave SC is placed in proximity with a topological insulator. Such a system can host edge states upon breaking of time-reversal symmetry, e.g., by introducing a magnetic vortex. This behavior was recently discovered to occur at surfaces of some materials, such as the iron-based SC $FeTe_{1-x}Se_x$ [77–82], and is anticipated in $PbSaTe_2$ [83], which thus makes these materials promising candidates for our purposes. Hence, our Hamiltonian may effectively describe the Majorana bound states on the surface of such materials when they are proximitized with a d-wave SC, either as a bilayer or as a Josephson coupling, as was suggested in Ref. [35]. We also point out that a proximity effect between niobium and graphene, through a single layer of chiral molecules, was demonstrated to display signatures which may be indicative of chiral p-wave superconductivity [84] and might provide additional means of realizing the model we studied here in the future.

Finally, we remark that a cuprate d-wave SC typically has a significantly larger critical temperature than the p-wave SCs discussed above. For instance, $YBa_2Cu_3O_{7-\delta}$ may reach $T_c \sim 100$ K [85], whereas $FeTe_{0.55}Se_{0.45}$ has $T_c \sim 15$ K [82], and T_c is doping dependent in both cases. Hence, the relative sizes of the two superconducting order parameters, Δ_p and Δ_d, might be tunable by changing the temperature and the doping. In any case, we hope that our findings will motivate further experimental efforts to demonstrate the tunability of the MZMs in mixed-pairing topological SCs by both the parent p-wave state and an external nonthermal tuning parameter, such as strain. Our results should also motivate further searches for material platforms where the proposed scenario can be relevant.

In closing, we point out that our mechanism may also be relevant for three-dimensional SCs which can be realized in doped octupolar (third-order) Dirac insulators, hosting corner MZMs [68]. This problem is, however, left for future investigation.

ACKNOWLEDGMENTS

M.A. thanks J. Danon for useful discussions. V.J. is grateful to B. Roy for useful discussions and the critical reading of the manuscript. The authors thank H. Roising for useful discussions. V.J. acknowledges support from the Swedish Research Council (Grant No. VR 2019-04735).

[1] A. Y. Kitaev, Unpaired Majorana fermions in quantum wires, Phys.-Usp. **44**, 131 (2001).

[2] N. Read and D. Green, Paired states of fermions in two dimensions with breaking of parity and time-reversal symmetries and the fractional quantum Hall effect, Phys. Rev. B **61**, 10267 (2000).

[3] M. Z. Hasan and C. L. Kane, Colloquium: Topological insulators, Rev. Mod. Phys. **82**, 3045 (2010).

[4] X.-L. Qi and S.-C. Zhang, Topological insulators and superconductors, Rev. Mod. Phys. **83**, 1057 (2011).

[5] Y. Tanaka, M. Sato, and N. Nagaosa, Symmetry and Topology in Superconductors–Odd-Frequency Pairing and Edge States–, J. Phys. Soc. Jpn. **81**, 011013 (2012).

[6] M. Leijnse and K. Flensberg, Introduction to topological superconductivity and Majorana fermions, Semicond. Sci. Technol. **27**, 124003 (2012).

[7] M. Sato and Y. Ando, Topological superconductors: A review, Rep. Prog. Phys **80**, 076501 (2017).

[8] J. Linder and A. V. Balatsky, Odd-frequency superconductivity, Rev. Mod. Phys. **91**, 045005 (2019).

[9] A. Y. Kitaev, Fault-tolerant quantum computation by anyons, Ann. Phys. (NY) **303**, 2 (2003).

[10] C. Nayak, S. H. Simon, A. Stern, M. H. Freedman, and S. Das Sarma, Non-Abelian anyons and topological quantum computation, Rev. Mod. Phys. **80**, 1083 (2008).

[11] R. Aguado and M. L. Kouwenhoven, Majorana qubits for topological quantum computing, Phys. Today **73**(66), 44 (2020).

[12] Y. Oreg and F. von Oppen, Majorana zero modes in networks of Cooper-pair boxes: Topologically ordered states and topological quantum computation, Annu. Rev. Condens. Matter Phys. **11**, 397 (2020).

[13] J. Alicea, New directions in the pursuit of Majorana fermions in solid state systems, Rep. Prog. Phys. **75**, 076501 (2012).

[14] C. W. J. Beenakker, Search for Majorana fermions in superconductors, Annu. Rev. Condens. Matter Phys. **4**, 113 (2013).

[15] S. Vijay and L. Fu, Teleportation-based quantum information processing with Majorana zero modes, Phys. Rev. B **94**, 235446 (2016).

[16] T. Karzig, C. Knapp, R. M. Lutchyn, P. Bonderson, M. B. Hastings, C. Nayak, J. Alicea, K. Flensberg, S. Plugge, Y. Oreg, C. M. Marcus, and M. H. Freedman, Scalable designs for quasiparticle-poisoning-protected topological quantum computation with Majorana zero modes, Phys. Rev. B **95**, 235305 (2017).

[17] S. Plugge, A. Rasmussen, R. Egger, and K. Flensberg, Majorana box qubits, New J. Phys. **19**, 012001 (2017).

[18] R. M. Lutchyn, E. P. A. M. Bakkers, L. P. Kouwenhoven, P. Krogstrup, C. M. Marcus, and Y. Oreg, Majorana zero modes in superconductor-semiconductor heterostructures, Nat. Rev. Mater. **3**, 52 (2018).

[19] A. Haim and Y. Oreg, Time-reversal-invariant topological superconductivity in one and two dimensions, Phys. Rep. **825**, 1 (2019).

[20] S. Park, H.-S. Sim, and P. Recher, Electron-Tunneling-Assisted Non-Abelian Braiding of Rotating Majorana Bound States, Phys. Rev. Lett. **125**, 187702 (2020).

[21] E. Prada, P. San-Jose, M. W. A. de Moor, A. Geresdi, E. J. H. Lee, J. Klinovaja, D. Loss, J. Nygård, R. Aguado, and L. P. Kouwenhoven, From Andreev to Majorana bound states in hybrid superconductor-semiconductor nanowires, Nat. Rev. Phys. **2**, 575 (2020).

[22] H.-L. Huang, M. Narożniak, F. Liang, Y. Zhao, A. D. Castellano, M. Gong, Y. Wu, S. Wang, J. Lin, Y. Xu, H. Deng, H. Rong, J. P. Dowling, C.-Z. Peng, T. Byrnes, X. Zhu, and J.-W. Pan, Emulating Quantum Teleportation of a Majorana Zero Mode Qubit, Phys. Rev. Lett. **126**, 090502 (2021).

[23] K. Flensberg, F. von Oppen, and A. Stern, Engineered platforms for topological superconductivity and Majorana zero modes, Nat. Rev. Mater. **6**, 944 (2021).

[24] W. A. Benalcazar, B. A. Bernevig, and T. L. Hughes, Quantized electric multipole insulators, Science **357**, 61 (2017).

[25] W. A. Benalcazar, B. A. Bernevig, and T. L. Hughes, Electric multipole moments, topological multipole moment pumping, and chiral hinge states in crystalline insulators, Phys. Rev. B **96**, 245115 (2017).

[26] Z. Song, Z. Fang, and C. Fang, $(d-2)$-Dimensional Edge States of Rotation Symmetry Protected Topological States, Phys. Rev. Lett. **119**, 246402 (2017).

[27] J. Langbehn, Y. Peng, L. Trifunovic, F. von Oppen, and P. W. Brouwer, Reflection-Symmetric Second-Order Topological Insulators and Superconductors, Phys. Rev. Lett. **119**, 246401 (2017).

[28] L. Li, M. Umer, and J. Gong, Direct prediction of corner state configurations from edge winding numbers in two- and three-dimensional chiral-symmetric lattice systems, Phys. Rev. B **98**, 205422 (2018).

[29] F. Schindler, Z. Wang, M. G. Vergniory, A. M. Cook, A. Murani, S. Sengupta, A. Y. Kasumov, R. Deblock, S. Jeon, I. Drozdov, H. Bouchiat, S. Guéron, A. Yazdani, B. A. Bernevig, and T. Neupert, Higher-order topology in bismuth, Nat. Phys. **14**, 918 (2018).

[30] E. Khalaf, Higher-order topological insulators and superconductors protected by inversion symmetry, Phys. Rev. B **97**, 205136 (2018).

[31] D. Călugăru, V. Juričić, and B. Roy, Higher-order topological phases: A general principle of construction, Phys. Rev. B **99**, 041301(R) (2019).

[32] D. Varjas, A. Lau, K. Pöyhönen, A. R. Akhmerov, D. I. Pikulin, and I. C. Fulga, Topological Phases without Crystalline Counterparts, Phys. Rev. Lett. **123**, 196401 (2019).

[33] A. Agarwala, V. Juričić, and B. Roy, Higher-order topological insulators in amorphous solids, Phys. Rev. Res. **2**, 012067(R) (2020).

[34] A. L. Szabó, R. Moessner, and B. Roy, Strain-engineered higher-order topological phases for spin-3/2 Luttinger fermions, Phys. Rev. B **101**, 121301(R) (2020).

[35] Y. Wang, M. Lin, and T. L. Hughes, Weak-pairing higher order topological superconductors, Phys. Rev. B **98**, 165144 (2018).

[36] Z. Wu, Z. Yan, and W. Huang, Higher-order topological superconductivity: Possible realization in Fermi gases and Sr_2RuO_4, Phys. Rev. B **99**, 020508(R) (2019).

[37] Q. Wang, C.-C. Liu, Y.-M. Lu, and F. Zhang, High-Temperature Majorana Corner States, Phys. Rev. Lett. **121**, 186801 (2018).

[38] Z. Yan, F. Song, and Z. Wang, Majorana Corner Modes in a High-Temperature Platform, Phys. Rev. Lett. **121**, 096803 (2018).

[39] X. Zhu, Tunable Majorana corner states in a two-dimensional second-order topological superconductor induced by magnetic fields, Phys. Rev. B **97**, 205134 (2018).

[40] Z. Yan, Higher-Order Topological Odd-Parity Superconductors, Phys. Rev. Lett. **123**, 177001 (2019).

[41] X. Zhu, Second-Order Topological Superconductors with Mixed Pairing, Phys. Rev. Lett. **122**, 236401 (2019).

[42] X.-H. Pan, K.-J. Yang, L. Chen, G. Xu, C.-X. Liu, and X. Liu, Lattice-Symmetry-Assisted Second-Order Topological Superconductors and Majorana Patterns, Phys. Rev. Lett. **123**, 156801 (2019).

[43] S. A. A. Ghorashi, X. Hu, T. L. Hughes, and E. Rossi, Second-order Dirac superconductors and magnetic field induced Majorana hinge modes, Phys. Rev. B **100**, 020509(R) (2019).

[44] B. Roy, Antiunitary symmetry protected higher-order topological phases, Phys. Rev. Res. **1**, 032048(R) (2019).

[45] S.-B. Zhang and B. Trauzettel, Detection of second-order topological superconductors by Josephson junctions, Phys. Rev. Res. **2**, 012018(R) (2020).

[46] J. Ahn and B.-J. Yang, Higher-order topological superconductivity of spin-polarized fermions, Phys. Rev. Res. **2**, 012060(R) (2020).

[47] R. W. Bomantara, Time-induced second-order topological superconductors, Phys. Rev. Res. **2**, 033495 (2020).

[48] B. Roy, Higher-order topological superconductors in $\mathcal{P}$-, $\mathcal{T}$-odd quadrupolar Dirac materials, Phys. Rev. B **101**, 220506(R) (2020).

[49] S.-B. Zhang, W. B. Rui, A. Calzona, S.-J. Choi, A. P. Schnyder, and B. Trauzettel, Topological and holonomic quantum computation based on second-order topological superconductors, Phys. Rev. Res. **2**, 043025 (2020).

[50] T. E. Pahomi, M. Sigrist, and A. A. Soluyanov, Braiding Majorana corner modes in a second-order topological superconductor, Phys. Rev. Res. **2**, 032068(R) (2020).

[51] X. Wu, W. A. Benalcazar, Y. Li, R. Thomale, C.-X. Liu, and J. Hu, Boundary-Obstructed Topological High-T_c Superconductivity in Iron Pnictides, Phys. Rev. X **10**, 041014 (2020) .

[52] A. Tiwari, A. Jahin, and Y. Wang, Chiral Dirac superconductors: Second-order and boundary-obstructed topology, Phys. Rev. Res. **2**, 043300 (2020).

[53] A. K. Ghosh, T. Nag, and A. Saha, Floquet generation of a second-order topological superconductor, Phys. Rev. B **103**, 045424 (2021).

[54] B. Fu, Z.-A. Hu, C.-A. Li, J. Li, and S.-Q. Shen, Chiral Majorana hinge modes in superconducting Dirac materials, Phys. Rev. B **103**, L180504 (2021).

[55] Y.-T. Hsu, W. S. Cole, R.-X. Zhang, and J. D. Sau, Inversion-Protected Higher-Order Topological Superconductivity in Monolayer WTe_2, Phys. Rev. Lett. **125**, 097001 (2020).

[56] C.-H. Hsu, P. Stano, J. Klinovaja, and D. Loss, Majorana Kramers Pairs in Higher-Order Topological Insulators, Phys. Rev. Lett. **121**, 196801 (2018).

[57] Z. Yan, Majorana corner and hinge modes in second-order topological insulator/superconductor heterostructures, Phys. Rev. B **100**, 205406 (2019).

[58] T. Liu, J. J. He, and F. Nori, Majorana corner states in a two-dimensional magnetic topological insulator on a high-temperature superconductor, Phys. Rev. B **98**, 245413 (2018).

[59] B. Jäck, Y. Xie, J. Li, S. Jeon, B. A. Bernevig, and A. Yazdani, Observation of a Majorana zero mode in a topologically protected edge channel, Science **364**, 1255 (2019).

[60] Y.-J. Wu, J. Hou, Y.-M. Li, X.-W. Luo, X. Shi, and C. Zhang, In-Plane Zeeman-Field-Induced Majorana Corner and Hinge Modes in an s-Wave Superconductor Heterostructure, Phys. Rev. Lett. **124**, 227001 (2020).

[61] M. Kheirkhah, Z. Yan, Y. Nagai, and F. Marsiglio, First- and Second-Order Topological Superconductivity and Temperature-Driven Topological Phase Transitions in the Extended Hubbard Model with Spin-Orbit Coupling Phys. Rev. Lett. **125**, 017001 (2020).

[62] S. Manna, P. Wei, Y. Xie, K. T. Law, P. A. Lee, and J. S. Moodera, Signature of a pair of Majorana zero modes in superconducting gold surface states, Proc. Natl. Acad. Sci. USA **117**, 8775 (2020).

[63] S. Ikegaya, W. B. Rui, D. Manske, and A. P. Schnyder, Tunable Majorana corner modes in noncentrosymmetric superconductors: Tunneling spectroscopy and edge imperfections, Phys. Rev. Res. **3**, 023007 (2021).

[64] Y. Volpez, D. Loss, and J. Klinovaja, Second-Order Topological Superconductivity in π-Junction Rashba Layers, Phys. Rev. Lett. **122**, 126402 (2019).

[65] S. Franca, D. V. Efremov, and I. C. Fulga, Phase-tunable second-order topological superconductor, Phys. Rev. B **100**, 075415 (2019).

[66] M. Kheirkhah, Z.-Y. Zhuang, J. Maciejko, and Z. Yan, Surface Bogoliubov-Dirac cones and helical Majorana hinge modes in superconducting Dirac semimetals, Phys. Rev. B **105**, 014509 (2022).

[67] A. K. Ghosh, T. Nag, and A. Saha, Hierarchy of higher-order topological superconductors in three dimensions, Phys. Rev. B **104**, 134508 (2021).

[68] B. Roy and V. Juričić, Mixed-parity octupolar pairing and corner Majorana modes in three dimensions, Phys. Rev. B **104**, L180503 (2021).

[69] T. Nag, V. Juričić, and B. Roy, Hierarchy of higher-order Floquet topological phases in three dimensions, Phys. Rev. B **103**, 115308 (2021).

[70] Notice that if we choose the d_{xy} component of the d-wave pairing, the corresponding domain wall is along the principal axes, $k_x = 0$, $k_y = 0$, and the corresponding zero modes are localized at the corners in an oblique (diamond)-square-lattice cut. See, for instance, Fig. 4(b) in Ref. [86], where the analogous corner zero modes are shown in the case of a second-order topological insulator.

[71] C. Lee, X. Wei, J. W. Kysar, and J. Hone, Measurement of the elastic properties and intrinsic strength of monolayer graphene, Science **321**, 385 (2008).

[72] C. C. Tsuei and J. R. Kirtley, Pairing symmetry in cuprate superconductors, Rev. Mod. Phys. **72**, 969 (2000).

[73] A. Pustogow, Y. Luo, A. Chronister, Y.-S. Su, D. A. Sokolov, F. Jerzembeck, A. P. Mackenzie, C. W. Hicks, N. Kikugawa, S. Raghu, E. D. Bauer, and S. E. Brown, Constraints on the superconducting order parameter in Sr_2RuO_4 from oxygen-17 nuclear magnetic resonance, Nature (London) **574**, 72 (2019).

[74] A. Chronister, A. Pustogow, N. Kikugawa, D. A. Sokolov, F. Jerzembeck, C. W. Hicks, A. P. Mackenzie, E. D. Bauer, and S. E. Brown, Evidence for even parity unconventional superconductivity in Sr_2RuO_4, Proc. Natl. Acad. Sci. USA **118**, e2025313118 (2021).

[75] L. Jiao, S. Howard, S. Ran, Z. Wang, J. O. Rodriguez, M. Sigrist, Z. Wang, N. P. Butch, and V. Madhavan, Chiral

superconductivity in heavy-fermion metal UTe_2, Nature (London) **579**, 523 (2020).

[76] L. Fu and C. L. Kane, Superconducting Proximity Effect and Majorana Fermions at the Surface of a Topological Insulator, Phys. Rev. Lett. **100**, 096407 (2008).

[77] G. Xu, B. Lian, P. Tang, X.-L. Qi, and S.-C. Zhang, Topological Superconductivity on the Surface of Fe-Based Superconductors, Phys. Rev. Lett. **117**, 047001 (2016).

[78] J. Wang and S.-C. Zhang, Topological states of condensed matter, Nat. Mater. **16**, 1062 (2017).

[79] T. Machida, Y. Sun, S. Pyon, S. Takeda, Y. Kohsaka, T. Hanaguri, T. Sasagawa, and T. Tamegai, Zero-energy vortex bound state in the superconducting topological surface state of Fe(Se, Te), Nat. Mater. **18**, 811 (2019).

[80] L. Kong, S. Zhu, M. Papaj, H. Chen, L. Cao, H. Isobe, Y. Xing, W. Liu, D. Wang, P. Fan, Y. Sun, S. Du, J. Schneeloch, R. Zhong, G. Gu, L. Fu, H.-J. Gao, and H. Ding, Half-integer level shift of vortex bound states in an iron-based superconductor, Nat. Phys. **15**, 1181 (2019).

[81] S. Zhu, L. Kong, L. Cao, H. Chen, M. Papaj, S. Du, Y. Xing, W. Liu, D. Wang, C. Shen, F. Yang, J. Schneeloch, R. Zhong, G. Gu, L. Fu, Y.-Y. Zhang, H. Ding, and H.-J. Gao, Nearly quantized conductance plateau of vortex zero mode in an iron-based superconductor, Science **367**, 189 (2020).

[82] P. Zhang, K. Yaji, T. Hashimoto, Y. Ota, T. K. Okazaki, Z. Wang, J. Wen, G. D. Gu, H. Ding, and S. Shin, Observation of topological superconductivity on the surface of an iron-based superconductor, Science **360**, 182 (2018).

[83] S.-Y. Guan, P.-J. Chen, and T.-M. Chuang, Topological surface states and superconductivity in non-centrosymmetric $PbTaSe_2$, Jpn. J. Appl. Phys. **60**, SE0803 (2021).

[84] N. Sukenik, H. Alpern, E. Katzir, S. Yochelis, O. Millo, and Y. Paltiel, Proximity effect through chiral molecules in Nb-graphene-based devices, Adv. Mater. Technol. **3**, 1700300 (2018).

[85] M. A. Hossain, J. D. F. Mottershead, D. Fournier, A. Bostwick, J. L. McChesney, E. Rotenberg, R. Liang, W. N. Hardy, G. A. Sawatzky, I. S. Elfimov, D. A. Bonn, and A. Damascelli, In situ doping control of the surface of high-temperature superconductors, Nat. Phys. **4**, 527 (2008).

[86] B. Roy and V. Juričić, Dislocation as a bulk probe of higher-order topological insulators, Phys. Rev. Res. **3**, 033107 (2021).